A Fast Diagnosis Method for Both IGBT Faults and Current Sensor Faults in Grid-Tied Three-Phase Inverters with Two Current Sensors

Zhan Li, *Student Member, IEEE*, Pat Wheeler, *Senior Member, IEEE*, Alan Watson, *Member, IEEE*, Alessandro Costabeber, *Member, IEEE*, Borong Wang, *Student Member, IEEE*, Yini Ren, *Student Member, IEEE*, Zhihong Bai, *Member, IEEE*, and Hao Ma, *Senior Member, IEEE*

***Abstract*- This paper considers fault detection in the case of a three-phase three-wire (3P3W) inverter, when only two current sensors are used to save cost or due to a faulty current sensor. With two current sensors, there is no current method addressing the diagnosis of both IGBT open-circuit (OC) faults and current sensor faults. In order to solve this problem, this paper proposes a method which innovatively combines two kinds of diagnosis variables, line voltage deviations and phase voltage deviations. The unique faulty characteristics of diagnosis variables for each fault are extracted and utilized to distinguish the fault. Using an average model, the method only needs the signals already available in the controller. Both IGBT OC faults and current sensor faults can be detected quickly in inverter mode and rectifier mode, so that the converter can be protected in a timely way to avoid further damages. In addition, error-adaptive thresholds are adopted to make the method robust. Effects such as system unbalance is analyzed to ensure that the method is robust and feasible. Simulation and experimental results are used to verify and validate the effectiveness of the method.**

NOMENCLATURE

v_{xy} (x,y =a,b,c)	Line voltages between phase X and phase Y
v_{xN}	Phase voltage of phase X
i_x	Current of phase X
V_{XY} (X,Y = A, B, C)	Bridge arm pole-to-pole voltage between phase X and phase Y
V_{XL}	Bridge arm pole voltage of phase X
V_{NL}	Voltage between output neutral point and lower point of DC bus
L_x	Filter inductance of phase X
R_x	Equivalent resistance of phase X
γ	Actual value of signal γ
γ^	Sampled value of signal γ
γ*	Estimated value of signal γ
$\Delta\gamma$^	Deviation between γ and γ^
$\Delta\gamma$*	Deviation between γ and γ*
$\bar{\gamma}[n]$	Average value of γ during $t[n\text{-}1]$ and $t[n]$
$\Delta V_{th,sub}$	Threshold of deviation ΔV_{sub}
Δ_{sub}	Polarity of deviation ΔV_{sub}
σ_γ	Error of signal or parameter γ
ξ_Γ	Calculation error of function Γ
$\xi_{\Delta v_{xN},IB}^{\wedge}$	The upper limit of the error caused by system unbalance calculated with sampled currents
$\xi_{\Delta v_{xN},IB}^{*}$	The upper limit of the error caused by system unbalance calculated with estimated voltages

Manuscript received May 14, 2019; revised August 19, 2019; accepted October 02, 2019. This work was supported by the National Nature Science Foundation of China under Grant 51337009. (*Corresponding author: Hao Ma.*)

Z. Li, B. Wang, Y. Ren, Z. Bai, and H. Ma are with the Institute of Power Electronics, College of Electrical Engineering, Zhejiang University, Hangzhou 310027, China (e-mail: lizhan@zju.edu.cn; borongw@126.com; 3130101062@zju.edu.cn; bai_zhihong@126.com; mahao@zju.edu.cn).

P. Wheeler and A. Watson are with the Power Electronics, Machines and Control Research Group, Department of Electrical and Electronic Engineering, University of Nottingham, Nottingham NG7 2RD, U.K. (e-mail: pat.wheeler@nottingham.ac.uk; alan.watson@nottingham.ac.uk).

A. Costabeber is with the Power Electronics Group, Department of Information Engineering, University of Padova, Padova 35131, Italy (e-mail: alessandro.costabeber@dei.unipd.it).

I. INTRODUCTION

Grid-tied three-phase voltage-source inverters are widely used in renewable energy systems, electrical traction systems, *etc*. Inverters play the key roles of interfaces controlling and transferring power. However, inverters are of the parts with highest failure rate [1]. Unexpected inverter failure may cause considerable loss; therefore, methods to improve inverter availability, protect systems, and reduce maintenance time are hot topics [2].

In inverters, power semiconductor switches, particularly IGBTs, are the most vulnerable devices [3]. IGBTs may suffer from short-circuit (SC) faults and open-circuit (OC) faults. Unlike SC fault protection, OC fault protection is not generally included as a standard feature in inverters. However, OC faults also cause malfunction and could lead to failures on other parts [4]. Therefore, it is useful to consider fast and accurate IGBT OC fault diagnosis methods. Many papers have been published focusing on IGBT OC fault diagnosis. These methods include data-driven methods and circuit-driven methods. The data-driven methods apply artificial intelligence algorithms [5]-[7] or advanced signal processing methods [8]-[10] to extract fault indication characteristics. The data-driven methods do not need circuit analysis or models, which makes them suitable for complicated systems. Nevertheless, they require large amounts of data and computational effort. Thus, for now, they are not good candidates for fast online inverter fault diagnosis. Circuit-driven methods can achieve faster fault

identification with less data, but they rely on circuit operation analysis or circuit models, so they are suitable for simpler and well-defined systems. Circuit-driven methods can be categorized as voltage signal based [11]-[14], current signal based [15]-[18] and model based [19]-[22]. With extra sampling and diagnosis circuits, voltage signal based methods introduced in [11]-[12] can detect the IGBT OC faults within one switching period. Current signal based methods [15]-[18] and model based methods [19]-[22] can diagnose IGBT OC faults with existing signals. Due to different features in terms of cost, speed, complexity and so on, these methods are favored in different applications.

As well as IGBT faults, inverters are also sensitive to sensor faults [23]. Sensor faults can be more catastrophic than IGBT OC faults. For example, when a fault occurs with a current sensor in grid-tied inverters, the current will rise quickly due to the actions of the close-loop control, which may cause further damages to IGBTs and sensitive loads. Therefore, it is necessary to diagnose sensor faults in a timely way. There have been some reports on fault diagnosis of sensors in inverters. Most of these methods are based on current analysis [24]-[26] and models [27]-[30]. Methods proposed in [24]-[25] are based on load current average values. They are simple and easy to implement. A fast and general method based on a parity space and temporal redundancies is developed in [26]. It is suitable for various kinds of sensor faults. Methods in [29]-[30] can handle multiple current sensor faults by utilizing current residuals generated by state observers.

Methods mentioned above show good performance in diagnosing IGBT OC faults or current sensor faults. However, the methods considering only one kind of fault may diagnose falsely when the other kind of fault occurs. IGBT faults and current sensor faults share faulty characteristics. Both faults can cause distortion in the sampled currents. This is why most diagnosis methods for only one kind of fault cannot work in an independent way, but interfere each other. As a result, the methods for IGBT fault diagnosis utilizing sampled currents may have false alarms when current sensor faults occur. On the other hand, the methods for current sensor faults are also interfered by IGBT faults. Therefore, in order to diagnose both faults accurately, it would be better to include both faults diagnosis in the same method. Besides, addressing two kinds of faults by one approach shows better simplicity in implementation than applying two separate methods, because the analysis, calculation and program codes of these two kinds of faults can be shared in part.

In recent years, some methods have been developed to consider both IGBT faults and sensor faults [31]-[33]. In [31], the current deviations generated by a Luenberger observer are used to diagnose both faults. In order to improve diagnosis speed, Ren *et al.* [32] proposed a method based on average bridge arm pole-to-pole voltage deviations. The method in [33] can diagnose multiple IGBT faults and current sensor faults through stator current analysis. In all these methods, the sum of three phase currents is used to distinguish IGBT faults from current sensor faults. Therefore, these methods are only suitable for the three-phase three-wire (3P3W) inverters with three current sensors.

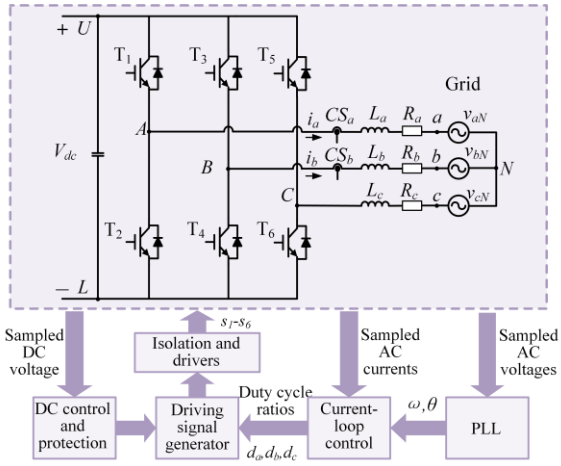

Fig.1 The grid-tied 3P3W inverter with two current sensors

The literature review shows the problem of diagnosing both IGBT OC faults and current sensor faults in 3P3W inverters with only two current sensors has not been investigated. In this paper, two kinds of diagnosis variables, line voltage deviations and phase voltage deviations, are innovatively combined to handle these two kinds of faults. The unique faulty characteristics of each fault is extracted and utilized to distinguish different faults. Importantly, the proposed method takes system unbalance into consideration. The problem of the system unbalance is new and inevitable when considering these two kinds of faults. It is solved by analyzing and computing the calculation error caused by the unbalance in two ways, so that the method is more robust and feasible.

This paper is organized as follows. The IGBT OC fault and current sensor fault analysis is given in section II. The proposed method is detailed in section III. Section IV discusses calculation errors analysis and thresholds selection. The simulation and experimental results are shown in section V and the conclusions are given in the last section.

II. Faulty Characteristics of Output Voltage Deviations

In this part, the deviation models of output line voltages and phase voltages are derived. The deviations are defined as

$$\Delta\gamma^* = \gamma - \gamma^*,\ \Delta\gamma^{\wedge} = \gamma - \gamma^{\wedge} \tag{1}$$

Where, γ is the actual value, γ^* and $\gamma^{\wedge}$ are the estimated and sampled values respectively.

Then, the output voltage deviation characteristics under different IGBT OC faults and current sensor faults are analyzed and summarized.

A. Output Voltage Deviation Models

Fig.1 shows a grid-tied 3P3W inverter with two current sensors. Two phase currents, three phase grid voltages and DC voltage are sampled for control.

Voltage sensors are healthy, so the actual output line voltages v_{xy} (x,y =a,b,c) can be considered the same as the sampled output line voltages $v_{xy}^{\wedge}$. Besides, according to the loop shown in Fig.2 and Kirchoff Voltage Law, there is

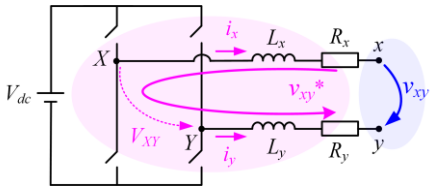

Fig.2 Loop for estimating output line voltages

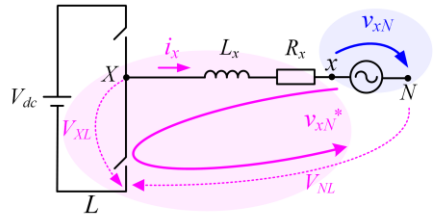

Fig.3 Loop for estimating output phase voltages

$$v_{xy} = -L_x \frac{di_x}{dt} - R_x i_x + V_{XY} + L_y \frac{di_y}{dt} + R_y i_y \tag{2}$$

Where $X,Y = A, B, C$. L_x is the filter inductance and R_x is the equivalent resistance.

Base on (2), the line voltage can be estimated as

$$v_{xy}^{*} = -L_x \frac{di_x^{\wedge}}{dt} - R_x i_x^{\wedge} + V_{XY}^{*} + L_y \frac{di_y^{\wedge}}{dt} + R_y i_y^{\wedge} \tag{3}$$

Where $i_x^{\wedge}$ is the sampled phase current, and V_{XY}^{*} is the estimated bridge arm pole-to-pole voltage.

Then (2) minus (3) gives the output line voltage deviation as

$$\Delta v_{xy}^{*} = -L_x \frac{d\Delta i_x^{\wedge}}{dt} - R_x \Delta i_x^{\wedge} + \Delta V_{XY}^{*} + L_y \frac{d\Delta i_y^{\wedge}}{dt} + R_y \Delta i_y^{\wedge} \tag{4}$$

Similarly, according to the loop shown in Fig. 3, there is

$$v_{xN} = -L_x \frac{di_x}{dt} - R_x i_x + V_{XL} - V_{NL} \tag{5}$$

Based on (5), there is

$$\sum_{x=a,b,c} v_{xN} = \sum_{x=a,b,c} (-L_x \frac{di_x}{dt} - R_x i_x) + \sum_{X=A,B,C} V_{XL} - 3V_{NL} \tag{6}$$

For a balanced system, where $L_a = L_b = L_c$, $R_a = R_b = R_c$, $v_{aN} + v_{bN} + v_{cN} = 0$, (6) becomes

$$V_{NL} = \frac{1}{3}(V_{AL} + V_{BL} + V_{CL}) \tag{7}$$

If the system is unbalanced, (7) is inaccurate. The error caused by system unbalance will be discussed in Section IV.

Similar to (4), the output phase voltage deviations are

$$\Delta v_{xN}^{*} = -L_x \frac{d\Delta i_x^{\wedge}}{dt} - R_x \Delta i_x^{\wedge} + \Delta V_{XL}^{*} - \Delta V_{NL}^{*} \tag{8}$$

Where

$$\Delta V_{NL}^{*} = \frac{1}{3}(\Delta V_{AL}^{*} + \Delta V_{BL}^{*} + \Delta V_{CL}^{*}) \tag{9}$$

B. Faulty Characteristics Analysis

When no fault occurs, $\Delta v_{xy}^{*} = 0$ and $\Delta v_{xN}^{*} = 0$. Whereas, when fault occurs, there may be $\Delta v_{xy}^{*} \neq 0$ and $\Delta v_{xN}^{*} \neq 0$. In this paper, the focused current sensor faults refer to open-circuit faults or short-circuit faults in sensor devices or conditioning circuits, as well as failures in A/D modules. In such faulty scenario, the output of the faulty sampled current is zero or other constants.

TABLE I
OUTPUT VOLTAGE DEVIATION CHARACTERISTICS OF DIFFERENT IGBT AND CURRENT SENSOR FAULTS IN 3P3W INVERTERS WITH TWO CURRENT SENSORS

Fault	Line voltage deviations			Phase voltage deviations		
	Δv_{ab}^{*}	Δv_{bc}^{*}	Δv_{ca}^{*}	Δv_{aN}^{*}	Δv_{bN}^{*}	Δv_{cN}^{*}
None	= 0	= 0	= 0	= 0	= 0	= 0
T_1	≤0	=0	≥0	≤0	≥0	≥0
T_2	≥0	=0	≤0	≥0	≤0	≤0
T_3	≥0	≤0	=0	≥0	≤0	≥0
T_4	≤0	≥0	=0	≤0	≥0	≤0
T_5	=0	≥0	≤0	≥0	≥0	≤0
T_6	=0	≤0	≥0	≤0	≤0	≥0
(CS_a×, CS_b)	≠0	≠0	≠0	≠0	=0	≠0
(CS_a, CS_b×)	≠0	≠0	≠0	= 0	≠0	≠0
(CS_a×, CS_c)	≠0	≠0	≠0	≠0	≠0	=0
(CS_a, CS_c×)	≠0	≠0	≠0	=0	≠0	≠0
(CS_b×, CS_c)	≠0	≠0	≠0	≠0	≠0	=0
(CS_b, CS_c×)	≠0	≠0	≠0	≠0	=0	≠0

Note: (CS_x×, CS_y) means current sensors CS_x and CS_y are available, where CS_x is faulty.

T_1 OC fault and sensor CS_a fault are taken as examples to analyze the faulty characteristics of output voltage deviations. It is considered that only one kind of fault occurs at a time.

When device T_1 OC fault occurs, according to the fault analysis in [22], there are $\Delta V_{AL}^{*} \leq 0$, $\Delta V_{BL}^{*} = 0$, $\Delta V_{CL}^{*} = 0$, $\Delta V_{AB}^{*} \leq 0$, $\Delta V_{BC}^{*} = 0$, $\Delta V_{CA}^{*} \geq 0$. Current sensors are healthy, namely $\Delta i_a^{\wedge} = 0$, $\Delta i_b^{\wedge} = 0$, $\Delta i_c^{\wedge} = -\Delta i_a^{\wedge} - \Delta i_b^{\wedge} = 0$. Then, according to (4) and (8), there are

$$\Delta v_{ab}^{*} \leq 0,\ \Delta v_{bc}^{*} = 0,\ \Delta v_{ca}^{*} \geq 0,\ \Delta v_{aN}^{*} \leq 0,\ \Delta v_{bN}^{*} \geq 0,\ \Delta v_{cN}^{*} \geq 0 \tag{10}$$

When sensor CS_a is faulty, there are $\Delta i_a^{\wedge} \neq 0$, $\Delta i_b^{\wedge} = 0$, $\Delta i_c^{\wedge} = -\Delta i_a^{\wedge} - \Delta i_b^{\wedge} \neq 0$. IGBTs are healthy, so $\Delta V_{AL}^{*} = 0$, $\Delta V_{BL}^{*} = 0$, $\Delta V_{CL}^{*} = 0$, $\Delta V_{AB}^{*} = 0$, $\Delta V_{BC}^{*} = 0$, $\Delta V_{CA}^{*} = 0$. Consequently

$$\Delta v_{ab}^{*} \neq 0,\ \Delta v_{bc}^{*} \neq 0,\ \Delta v_{ca}^{*} \neq 0,\ \Delta v_{aN}^{*} \neq 0,\ \Delta v_{bN}^{*} = 0,\ \Delta v_{cN}^{*} \neq 0 \tag{11}$$

With similar analysis, all faulty characteristics of output voltage deviations for different faults can be extracted and concluded in TABLE I. In the table, the cases where current sensors are in other phases are also included. For example, (CS_a×, CS_c) indicates the case where current sensors are in phase A and phase C, and the sensor in phase A CS_a is faulty.

III. PROPOSED FAULT DIAGNOSIS METHOD

A. Basic Principle of the Diagnosis Method

It can be observed from TABLE I that, line voltage deviations or phase voltage deviations alone are not adequate for distinguishing IGBT OC faults from current sensor faults. However, the combinations of output line and phase voltage deviations show unique characteristics for each fault. Therefore, it is proposed that two kinds of faulty

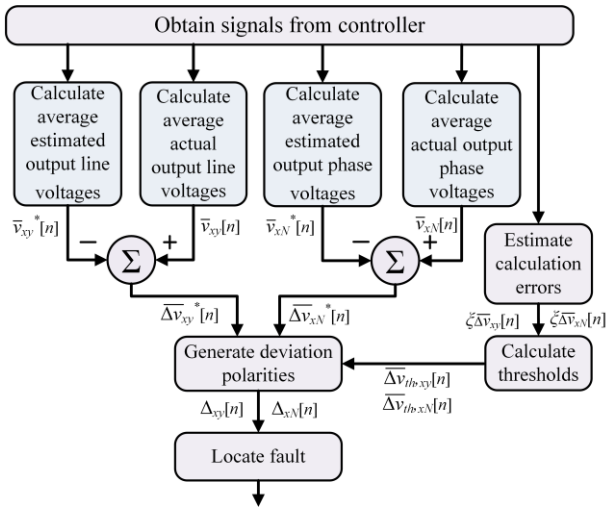

Fig.4 Principle of the proposed fault diagnosis method

characteristics are combined for fault identification. In order to utilize only existing signals in the controller, especially for a common circumstance where signals are sampled every switching period, the average model is applied to calculate output voltage deviations.

The average model can be defined as

$$\bar{\gamma}[n]=\frac{1}{T_S}\int_{t[n-1]}^{t[n]}\gamma dt \tag{12}$$

Where T_S is the sampling period. The sampling frequency can be different from the switching frequency. In this paper, as in most cases, the sampling frequency equals switching frequency.

The diagnosis principle is shown in Fig.4. The average output line and phase voltage deviations are taken as diagnosis variables. The calculation models of diagnosis variables will be given later. Ideally, the deviations should be zero when no fault occurs. However due to calculation error caused by sampling error, inductance error, system unbalance, *etc.*, the deviations are not always exactly zero under normal operation. Therefore, for robustness purposes, the error-adaptive threshold method proposed in [22] is applied in this method, which will be detailed in section IV.

After obtaining the thresholds, the deviation polarities $\Delta_{xy}[n]$ and $\Delta_{xN}[n]$ can be determined as

$$\Delta_{sub}=\begin{cases}P, & \Delta V_{sub}\geq\Delta V_{th,sub}\\ Z, & -\Delta V_{th,sub}<\Delta V_{sub}<\Delta V_{th,sub}\\ N, & \Delta V_{sub}\leq-\Delta V_{th,sub}\end{cases} \tag{13}$$

Then, according to the faulty characteristics shown in TABLE I, the criteria for diagnosing IGBT OC fault and current sensor fault are given in TABLE II.

In order to further improve robustness against disturbances, like noise and unmodeled high harmonics, the minimum time judging rule is implemented. The fault diagnosis result has to remain for the minimum time T_{min} to be considered reliable. The higher T_{min} leads to the better robustness and but longer detection time. In this paper, T_{min} is set to $2T_S$. Besides, the signal filters in the conditioning circuirts and software are also

TABLE II
CRITERIA FOR IGBT AND CURRENT SENSOR FAULT DIAGNOSIS FOR 3P3W INVERTER WITH TWO CURRENT SENSORS

Fault	Line voltage deviation polarities			Phase voltage deviation polarities		
	Δ_{ab}	Δ_{bc}	Δ_{ca}	Δ_{aN}	Δ_{bN}	Δ_{cN}
None	Z	Z	Z	Z	Z	Z
T_1	N	Z	P	N	P	P
T_2	P	Z	N	P	N	N
T_3	P	N	Z	P	N	P
T_4	N	P	Z	N	P	N
T_5	Z	P	N	P	P	N
T_6	Z	N	P	N	N	P
(CS_a×, CS_b)	P/N	P/N	P/N	P/N	Z	P/N
(CS_a, CS_b×)	P/N	P/N	P/N	Z	P/N	P/N
(CS_a×, CS_c)	P/N	P/N	P/N	P/N	P/N	Z
(CS_a, CS_c×)	P/N	P/N	P/N	Z	P/N	P/N
(CS_b×, CS_c)	P/N	P/N	P/N	P/N	P/N	Z
(CS_b, CS_c×)	P/N	P/N	P/N	P/N	Z	P/N

Note: "/" means "or".

helpful for eliminating the effects of disturbances. In the experiments, the harware filters are applied.

B. Calculation of Average Output Voltage Deviations

According to (3) and (12), the average estimated output line voltages can be calculated as

$$\begin{aligned}\bar{v}_{xy}^{*}[n]=&-\frac{L_x}{T_S}(i_x\hat{}[n]-i_x\hat{}[n-1])-\frac{R_x}{2}(i_x\hat{}[n]+i_x\hat{}[n-1])+\bar{V}_{xy}^{*}[n]\\&+\frac{L_y}{T_S}(i_y\hat{}[n]-i_y\hat{}[n-1])+\frac{R_y}{2}(i_y\hat{}[n]+i_y\hat{}[n-1])\end{aligned} \tag{14}$$

Where

$$\bar{V}_{xY}^{*}[n]=\frac{1}{2}(V_{dc}\hat{}[n-1]+V_{dc}\hat{}[n])(d_x[n-1]-d_y[n-1]) \tag{15}$$

The voltage sensors are healthy, so the actual output line voltage can be obtained as

$$\bar{v}_{xy}[n]=\frac{1}{2}(v_{xy}\hat{}[n-1]+v_{xy}\hat{}[n]) \tag{16}$$

Similarly, the average estimated and actual output phase voltages are

$$\bar{v}_{xN}^{*}[n]=-\frac{L_x}{T_S}(i_x\hat{}[n]-i_x\hat{}[n-1])-\frac{R_x}{2}(i_x\hat{}[n]+i_x\hat{}[n-1])+\bar{V}_{xL}^{*}[n]-\bar{V}_{NL}^{*}[n] \tag{17}$$

$$\bar{v}_{xN}[n]=\frac{1}{2}(v_{xN}\hat{}[n-1]+v_{xN}\hat{}[n]) \tag{18}$$

Where

$$\bar{V}_{xL}^{*}[n]=\frac{1}{2}(V_{dc}\hat{}[n-1]+V_{dc}\hat{}[n])\cdot d_x[n-1] \tag{19}$$

$$\bar{V}_{NL}^{*}[n]=\frac{1}{6}(V_{dc}\hat{}[n-1]+V_{dc}\hat{}[n])\cdot\sum_{x=a,b,c}d_x[n-1] \tag{20}$$

More detailed derivation of the calculation model can be found in [22].

Finally, the average output voltage deviations are

$$\overline{\Delta v}_{xy}[n]=\bar{v}_{xy}[n]-\bar{v}_{xy}^{*}[n] \tag{21}$$

$$\overline{\Delta v}_{xN}[n]=\bar{v}_{xN}[n]-\bar{v}_{xN}^{*}[n] \tag{22}$$

In implementation, the calculation can be furtherly simplified. For example, $\overline{\Delta v}_{xy}[n]$ can be calculated directly by $\overline{\Delta v}_{xy}[n]=\overline{\Delta v}_{xN}[n]-\overline{\Delta v}_{yN}[n]$ rather than by (14)-(16).

IV. Error Analysis and Thresholds Selection

A. Errors Caused by System Unbalance

For an unbalanced system, (7) is not accurate, which results in calculation errors in the output phase voltage deviations. The error caused by system unbalance $\xi_{\Delta v_{xN},IB}$ can be defined as

$$\xi_{\Delta v_{xN},IB}=V_{NL}-\frac{1}{3}(V_{AL}+V_{BL}+V_{CL}) \tag{23}$$

It can be obtained from (6) that

$$\xi_{\Delta v_{xN},IB}=\frac{1}{3}\sum_{x=a,b,c}(-L_x\frac{di_x}{dt}-R_x i_x-v_{xN}) \tag{24}$$

Normally, R_a, R_b, R_c are small and similar thus (24) can be simplified as

$$\xi_{\Delta v_{xN},IB}=\frac{1}{3}\sum_{x=a,b,c}(-L_x\frac{di_x}{dt}-v_{xN}) \tag{25}$$

Considering only current sensors CS_a and CS_b are available, by replacing i_c with $(-i_a-i_b)$, (25) can be written as

$$\xi_{\Delta v_{xN},IB}=\frac{1}{3}((L_c-L_a)\frac{di_a}{dt}+(L_c-L_b)\frac{di_b}{dt}-\sum_{x=a,b,c}v_{xN}) \tag{26}$$

Two methods are developed to estimate the upper limit of $\xi_{\Delta v_{xN},IB}$ corresponding to two circumstances: when current sensors are healthy, and when current sensors are faulty (IGBTs are healthy).

1) When current sensors are healthy

Define ΔL as the maximum inductance unbalance, namely $L\in[L-\Delta L, L+\Delta L]$. According to (26), there is

$$\xi_{\Delta v_{xN},IB}\le\frac{1}{3}(2\Delta L|\frac{di_a}{dt}|+2\Delta L|\frac{di_b}{dt}|+|\sum_{x=a,b,c}v_{xN}|) \tag{27}$$

Then the upper limit of $\xi_{\Delta v_{xN},IB}$ can be calculated with sampled currents, which is denoted as $\hat{\xi}_{\Delta v_{xN},IB}$.

$$\hat{\xi}_{\Delta v_{xN},IB}=\frac{1}{3}(2\Delta L|\frac{d\hat{i}_a}{dt}|+2\Delta L|\frac{d\hat{i}_b}{dt}|+|\sum_{x=a,b,c}\hat{v}_{xN}|) \tag{28}$$

After averaging

$$\hat{\bar{\xi}}_{\Delta v_{xN},IB}[n]=\frac{1}{3}(2\Delta L|\frac{\hat{i}_a[n]-\hat{i}_a[n-1]}{T_S}|+2\Delta L|\frac{\hat{i}_b[n]-\hat{i}_b[n-1]}{T_S}|+|\sum_{x=a,b,c}\hat{\bar{v}}_{xN}[n]|) \tag{29}$$

2) When current sensors are faulty

When current sensors are faulty, $\hat{\xi}_{\Delta v_{xN},IB}$ may be lower than the actual error $\xi_{\Delta v_{xN},IB}$. Therefore, the second method based on estimated voltages rather than sampled currents is developed. The error calculated with estimated voltages is denoted as $\xi^*_{\Delta v_{xN},IB}$.

According to Kirchhoff Voltage Law, there is

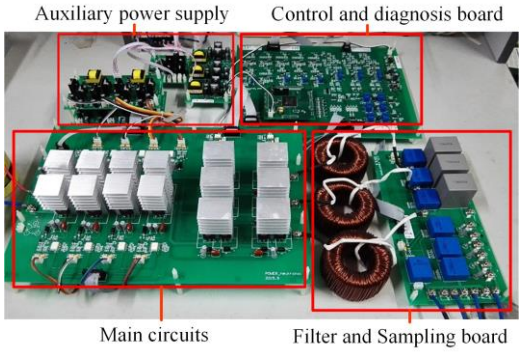

Fig.5 Experimental setup

TABLE III
Specification of the Inverter in Simulations and Experiments

Parameters	Symbols	Value
DC-link voltage	V_{dc}	400V
Grid phase voltages	v_{xN}	110V(rms), 50Hz
Rated power	P_{rate}	1.2kW
Filter inductances	L_a, L_b, L_c	8.5mH, 9.5mH, 9.5mH
Equivalent resistances	R_a, R_b, R_c	0.3Ω, 0.3Ω, 0.3Ω
Switching/Sampling frequency	f_s	10kHz
Sampling error of V_{dc}, v_{xy}, v_{xN}, i_x	σ_{Vdc},σ_{vxy}, σ_{vxN}, σ_{ix}	4V, 4V, 2V, 0.06A
Inductance error	σ_{Lf}	1.8mH
Dead time	T_{DD}	1.5μs
Delay time	T_{DL}	1μs

$$\begin{cases} V_{AB}-v_{ab}=L_a\frac{di_a}{dt}+R_a i_a-L_b\frac{di_b}{dt}-R_b i_b \\ V_{AC}-v_{ac}=L_a\frac{di_a}{dt}+R_a i_a+L_c\frac{d(i_a+i_b)}{dt}-R_c i_c \end{cases} \tag{30}$$

Then it can be derived from (30) that

$$\begin{aligned}(L_c-L_a)\frac{di_a}{dt}+(L_c-L_b)\frac{di_b}{dt}=&\underbrace{\frac{(L_c-L_a)L_b+(L_c-L_b)L_a}{L_aL_b+L_bL_c+L_aL_c}}_{\text{PART 1}}\underbrace{(V_{AC}-v_{ac})}_{\text{PART 2}}\\&+\underbrace{(\frac{(L_c-L_a)L_b+(L_c-L_b)L_a}{L_aL_b+L_bL_c+L_aL_c}\frac{L_c}{L_b}-\frac{(L_c-L_a)}{L_a})}_{\text{PART 3}}\underbrace{(V_{AB}-v_{ab})}_{\text{PART 4}}\\&+\underbrace{\frac{(L_c-L_a)L_b+(L_c-L_b)L_a}{L_aL_b+L_bL_c+L_aL_c}(\frac{L_b}{L_c}(R_a i_a-R_c i_c)+R_a i_a-R_b i_b))+\frac{(L_c-L_b)}{L_b}(R_a i_a-R_b i_b)}_{\text{PART 5}}\end{aligned} \tag{31}$$

There are five parts in (31). The maximum values of PART 1, PART 3 and PART 5 can be obtained easily with the nonlinear programming tool in MATLAB. An example is given below. The parameters in the simulation and experiments are applied in this example, which is shown in TABLE III. ΔL= 5.5%L, R_a= R_b = R_c =0.3Ω, $i_x\in$[–10A, 10A]. Then it can be obtained that PART 1 ≤ 0.0747, PART 3 ≤ 0.0683, PART 5 ≤ 1.29V. Thus

$$|(L_c-L_a)\frac{di_a}{dt}+(L_c-L_b)\frac{di_b}{dt}|\le 0.0747|V_{AC}-v_{ac}|+0.0683|V_{AB}-v_{ab}|+1.29\text{V} \tag{32}$$

Finally

$$\xi^*_{\Delta v_{xN},IB}=\frac{1}{3}(0.0747|V_{AC}^*-\hat{v}_{ac}|+0.0683|V_{AB}^*-\hat{v}_{ab}|+1.29\text{V}+|\sum_{x=a,b,c}\hat{v}_{xN}|) \tag{33}$$

After averaging

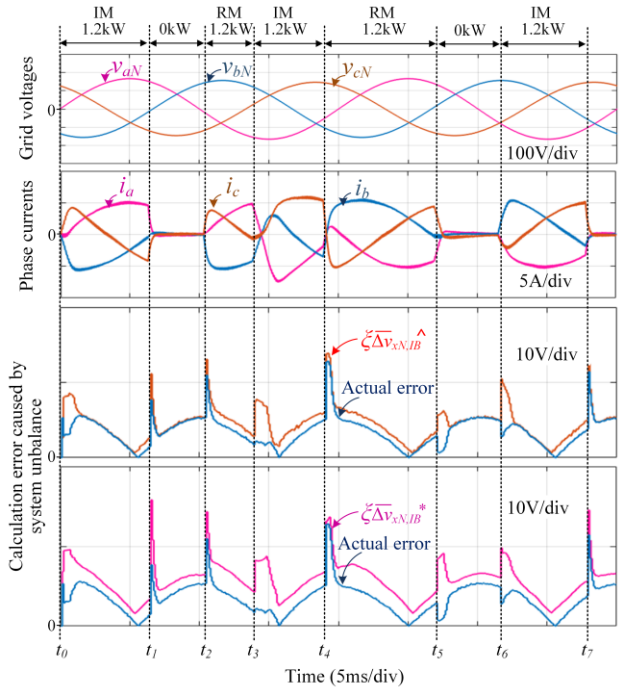

Fig.6 Simulation waveforms under power changes

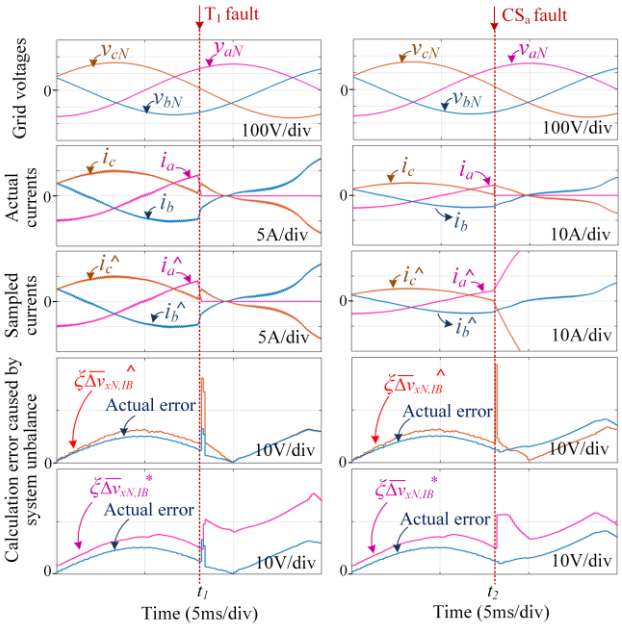

Fig.7 Simulation waveforms when T_1 OC fault or CS_a fault occurs

$$\xi_{\overline{\Delta v}xN,IB}{}^{*}[n]=\frac{1}{3}(0.0747|\overline{V}_{AC}{}^{*}[n]-\overline{v}_{ac}{}^{\wedge}[n]| +0.0683|\overline{V}_{AB}{}^{*}[n]-\overline{v}_{ab}{}^{\wedge}[n]|+1.29\mathrm{V}+|\sum_{x=a,b,c}\overline{v}_{xN}{}^{\wedge}[n]|) \quad (34)$$

In conclusion, when current sensors are healthy, $\xi_{\overline{\Delta v}xN,IB}{}^{\wedge}[n]$ calculated by (29) must be higher than the actual error; when current sensors are faulty, $\xi_{\overline{\Delta v}xN,IB}{}^{*}[n]$ calculated by (34) must be higher than the actual error. Therefore, $\xi_{\overline{\Delta v}xN,IB}[n]$ is chosen as

$$\xi_{\overline{\Delta v}xN,IB}[n]=\max\{\xi_{\overline{\Delta v}xN,IB}{}^{\wedge}[n],\ \xi_{\overline{\Delta v}xN,IB}{}^{*}[n]\} \quad (35)$$

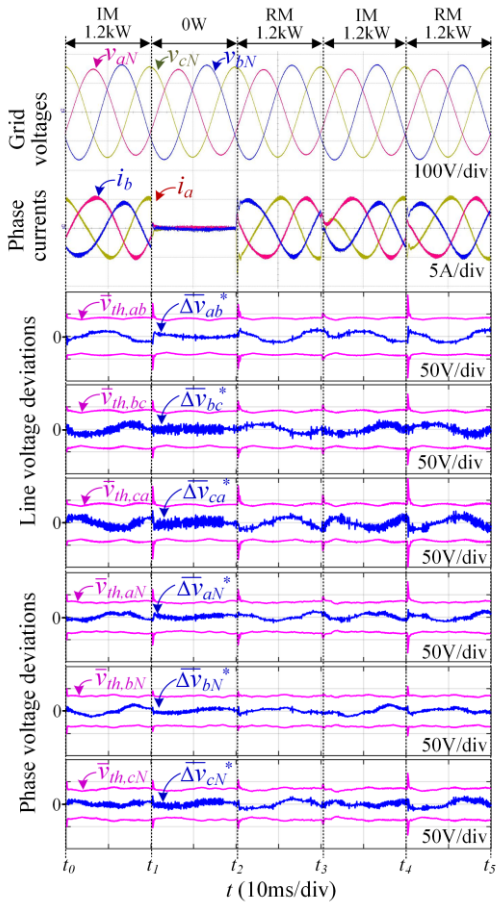

Fig.8 Experimental waveforms under power changes

B. *Modeling Errors*

Beside system unbalance, the calculation errors can be caused by modeling errors from other factors, including sampling error, inductance error, dead time and delay time.

Define function Γ as

$$\Gamma=f(\gamma_1,...,\gamma_k) \quad (36)$$

Where γ_1,.. γ_k are sampled signals and model parameters.

Define $\sigma_{\gamma 1,..}$ $\sigma_{\gamma k,}$ as the maximum errors of γ_1,..γ_k. Then the total error of Γ, namely ξ_Γ, caused by errors $\sigma_{\gamma 1,..}$ σ_γ can be estimated as

$$\xi_\Gamma=\sum_{i=1}^{i=k}|\frac{d_\Gamma}{d\gamma_i}\cdot\sigma_{\gamma_i}| \quad (37)$$

In the derived calculation model, sampling errors and parameter errors are the factors causing modeling errors. According to (37), (14)-(22), the total calculation error of diagnosis variables from sampling and parameter errors are

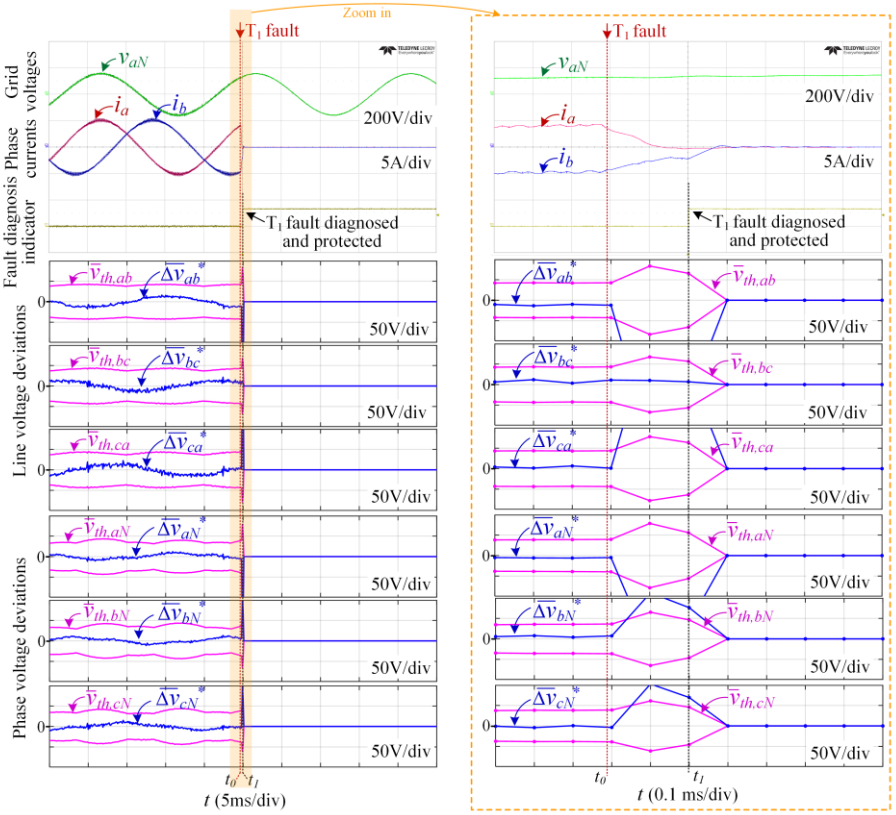

Fig.9 Experimental waveforms of T_1 OC fault diagnosis in inverter mode

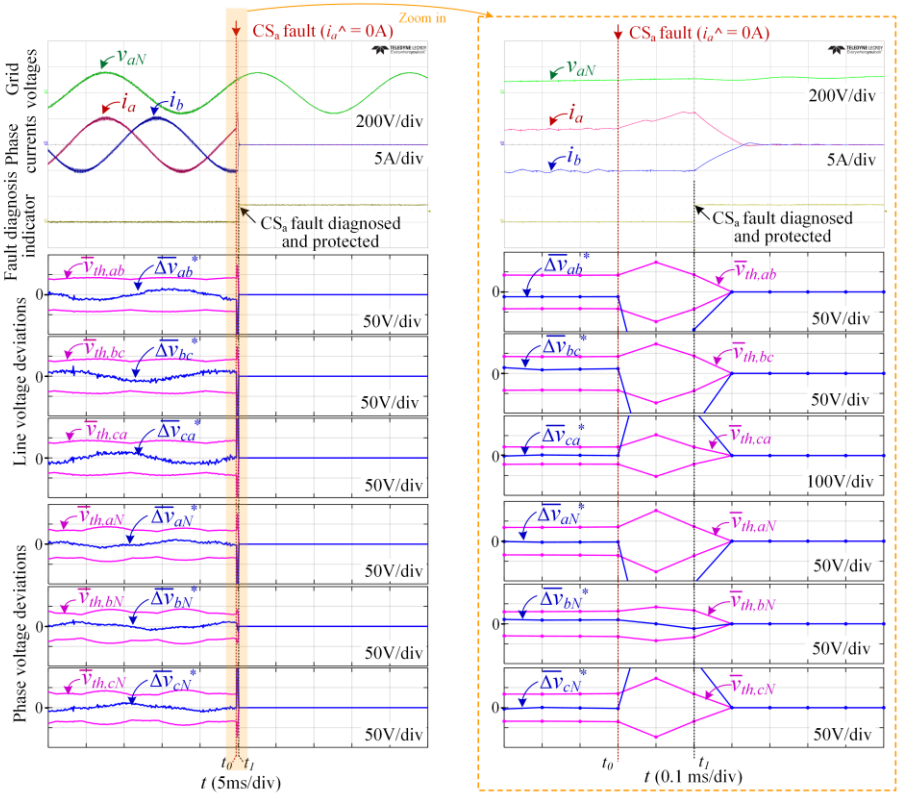

Fig.10 Experimental waveforms of CS_a fault diagnosis in inverter mode

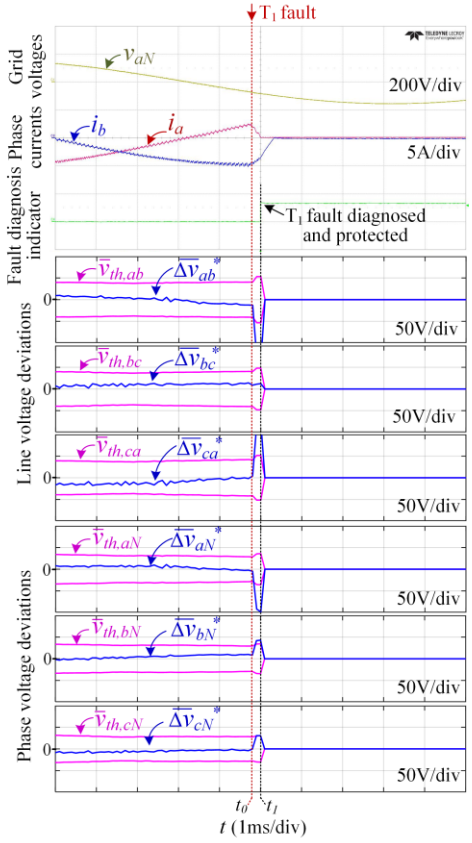

Fig.11 Experimental waveforms of T_1 OC fault diagnosis in rectifier mode

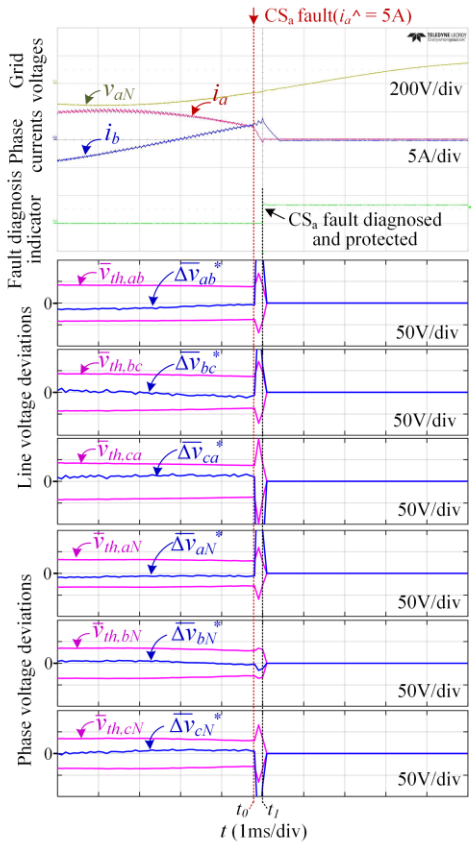

Fig.12 Experimental waveforms of CS_a fault diagnosis in rectifier mode

$$\xi_{\overline{\Delta v}_{xy},SP}[n]=\frac{1}{T_S}\sigma_{L_f}\left(\left|i_x\hat{}[n]-i_x\hat{}[n-1]\right|\right)+\frac{1}{T_S}\sigma_{L_f}\left(\left|i_y\hat{}[n]-i_y\hat{}[n-1]\right|\right)$$
$$+\sigma_{V_{dc}}\left(\left|d_x[n-1]-d_y[n-1]\right|\right)+\sigma_{v_{xy}}+\frac{4}{T_S}\sigma_{i_x}L_f \quad (38)$$

$$\xi_{\overline{\Delta v}_{xN},SP}[n]=\frac{1}{T_S}\sigma_{L_f}\left(\left|i_x\hat{}[n]-i_x\hat{}[n-1]\right|\right)+\sigma_{V_{dc}}\left(\left|d_x[n-1]\right.\right.$$
$$\left.\left.-\frac{1}{3}\left|\sum_{x=a,b,c}d_x[n-1]\right|\right)+\sigma_{v_{xN}}+\frac{2}{T_S}\sigma_{i_x}L_f \quad (39)$$

Where σ_{Lf} is the maximum inductance error, σ_{Vdc}, σ_{vxy}, σ_{vxN}, σ_{ix} are the maximum sampling errors of V_{dc}, v_{xy}, v_{xN}, i_x. The determination of sampling errors and inductance error is explained in [34].

Beside sampling errors and parameter errors, dead time and delay time can also cause modeling errors. The impacts of the dead time and the delay time are discussed in [22]. In this manuscript the maximum calculation errors from dead time T_{DD} and delay time T_{DL} can be obtained as

$$\xi_{\overline{\Delta v}_{xy},DD}=2V_{dc}\cdot\frac{T_{DD}}{T_S},\quad \xi_{\overline{\Delta v}_{xN},DD}=\frac{4}{3}V_{dc}\cdot\frac{T_{DD}}{T_S} \quad (40)$$

$$\xi_{\overline{\Delta v}_{xy},DL}=2V_{dc}\cdot\frac{T_{DL}}{T_S},\quad \xi_{\overline{\Delta v}_{xN},DL}=2V_{dc}\cdot\frac{T_{DL}}{T_S} \quad (41)$$

C. Thresholds Selection

After obtaining the calculation errors, the thresholds $\overline{\Delta v}_{th,xy}[n]$ and $\overline{\Delta v}_{th,xN}[n]$ can be selected as

$$\overline{\Delta v}_{th,xy}[n]=\xi_{\overline{\Delta v}_{xy},SP}[n]+\xi_{\overline{\Delta v}_{xy},DD}+\xi_{\overline{\Delta v}_{xy},DL} \quad (42)$$

$$\overline{\Delta v}_{th,xN}[n]=\xi_{\overline{\Delta v}_{xN},IB}[n]+\xi_{\overline{\Delta v}_{xN},SP}[n]+\xi_{\overline{\Delta v}_{xN},DD}+\xi_{\overline{\Delta v}_{xN},DL} \quad (43)$$

IV. Simulation and Experimental Results

Simulation and experimental results have been obtained to verify the correctness and effectiveness of the proposed method. The specification of the 3P3W inverter for simulations and experiments is given in TABLE III. Fig.5 shows the experimental platform. The system control and fault diagnosis methodologies are implemented using TMS320F28335 DSP. In the experiments, the IGBT OC fault is simulated by removing the corresponding driver signal. The current sensor fault is simulated by setting the faulty sampled current to 0A or 5A.The fault diagnosis indicator signals are given by outputs on the DSP I/O pins.

A. Simulation Verification of System Unbalance Error Analysis

Simulations in this section aim to verify the theoretical correctness of the calculation error caused by system unbalance. In the simulations, the filter inductances (L_a, L_b, L_c)

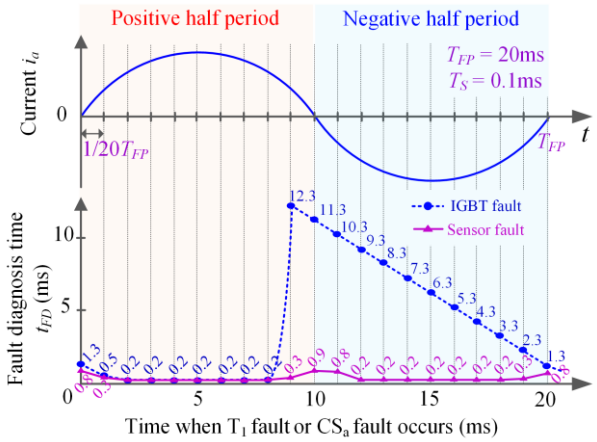

Fig. 13 Diagnosis time when T_1 fault or CS_a fault occurs at 20 evenly-spaced moments in a fundamental period

are (8.5mH, 9.5mH, 9.5mH), with ΔL of 0.5mH. The grid voltages are unbalanced by 5%. Current waveforms are also unbalanced.

In Fig.6, power is varied between 1.2kW in inverter mode (IM) and 1.2kW in rectifier mode (RM) several times. It can be observed that the calculation error caused by inductance unbalance is high when power changes drastically, namely, when *di/dt* is high. This is in accordance with (26). The result shows both $\hat{\xi}_{\overline{\Delta vxN},IB}$ and $\xi^{*}_{\overline{\Delta vxN},IB}$ are always higher than the actual error when no fault occurs.

Fig.7 shows the simulation results when T_1 OC fault or CS_a fault occurs. At t_1, the IGBT T_1 fault occurs. Before and after the T_1 fault, $\hat{\xi}_{\overline{\Delta vxN},IB}$ is always higher than the actual error. Whereas, $\xi^{*}_{\overline{\Delta vxN},IB}$ is lower than the actual error at t_1. The current sensor CS_a fault occurs at t_2. Before and after CS_a fault, $\xi^{*}_{\overline{\Delta vxN},IB}$ is always higher than the actual error. However, $\hat{\xi}_{\overline{\Delta vxN},IB}$ is lower than the actual error after CS_a fault. These observations are the same as the error analysis.

The simulation results show that the analysis of the calculation error caused by system unbalance is correct. (35) can be used to make sure that the estimated calculation error caused by system unbalance is higher than the actual error.

B. *Experimental Result of Robustness*

Fig.8 shows the experimental results under normal operation with power changes ranging from 1.2kW in RM to 1.2kW in IM. In this experiment, the filter inductances (L_a, L_b, L_c) are (8.5mH, 9.5mH, 9.5mH), with ΔL of 0.5mH. The grid voltages are unbalanced by 5% and the current waveforms are also unbalanced. It can be observed that with various power rates and under drastic power changes *at* t_1-t_4, all the diagnosis variables are within thresholds. No false diagnosis is caused. These experimental results prove this method is featured with strong resistance against system unbalance, modeling errors and power changes.

C. *Experimental Results of IGBT Fault and Current Sensor Fault Diagnosis*

Fig.9 shows the experimental waveforms of IGBT T_1 OC fault diagnosis. Before the fault occurs, all the diagnosis variables are within the thresholds. After the fault is triggered at t_0, the voltage deviation polarities (Δ_{ab}, Δ_{bc}, Δ_{ca}, Δ_{aN}, Δ_{bN}, Δ_{cN}) change to (N, Z, P, N, P, P) soon. According to the criteria in TABLE II, T_1 OC fault is diagnosed at t_1. The fault diagnosis time is 0.2ms (two switching periods).

Fig.10 demonstrates the result of current sensor CS_a fault diagnosis. The current sensor fault is triggered at t_0, then the voltage deviation polarities change to (N, N, P, N, Z, P) soon. According to the criteria in TABLE II, CS_a fault is diagnosed at t_1. The fault diagnosis time is 0.2ms (two switching periods).

Similar experiments have been carried out in rectifier mode, as shown in Fig.11 and Fig.12. It can be seen that the performance in rectifier mode is the same as in inverter mode. Both faults are diagnosed in two switching periods.

These experiments verify the proposed method can diagnose the IGBT OC faults and current sensor faults accurately and quickly in both inverter mode and rectifier mode.

D. *Experimental Diagnosis Speed*

In order to give an overview of the diagnosis speed, the diagnosis time of IGBT faults and current sensor faults during a fundamental period is investigated and shown in Fig.13. The diagnosis time is obtained by experiments in inverter mode.

It can be seen that, the diagnosis time of IGBT T_1 fault is short in the positive half period, about 0.2ms (two switching periods, 1% fundamental period). However if T_1 fault occurs in the negative half period, the fault cannot be detected immediately but until the next positive half period comes. This is because T_1 fault does not affect the operation of inverter in the negative half periods. During the whole fundamental period, the fault diagnosis time of current sensor CS_a fault is short. Most diagnosis time is 0.2ms (two switching periods, 1% fundamental period).

In conclusion, this method shows outstanding performance in terms of diagnosis speed.

V. CONCLUSION

The contributions of this paper can be concluded as:

1) A new method is proposed. Two kinds of diagnosis variables, line voltage deviations and phase voltage deviations, are innovatively combined to handle two kinds of faults. The unique faulty characteristics of each fault is extracted and utilized to distinguish the fault. The method of combining various kinds of diagnosis variables for multiple kinds of faults may help stimulate new ideas.

2) The proposed method is the only method so far that can diagnose both IGBT OC fault and current sensor fault in the grid-tied 3P3W inverter with only two current sensors by utilizing signals already existing in the controller. The fault can be detected in 0.2ms (two switching periods, 1% fundamental period) at the fastest in inverter and rectifier

modes, which enables the converter to be protected in a timely way to avoid further damages.

3) The problem of the system unbalance is solved by computing the calculation error caused by the unbalance in two ways, so that the method is more robust and feasible. The idea of tackling non-ideal factors to make a proposed method more practically valuable is interesting and helpful to researchers and engineers.

It should be noted that this method may have some limitations. It can only handle single IGBT OC fault or current sensor fault. It is best effective for current sensor faults which cause the sampled current to be zero or other constants. Other kinds of current sensor faults will be covered in the future work.

REFERENCES

[1] B. Hahn, M. Durstewitz, K. Rohrig, "Reliability of wind turbines - Experience of 15 years with 1500 WTs", *Wind Energy: Proceedings of the Euromech Colloquium*, Springer-Verlag, Berlin. 2007, pp. 329-332.

[2] Wang H, Liserre M, Blaabjerg F. "Toward reliable power electronics: Challenges design tools and opportunities". *IEEE Industrial Electronics Magazine*, vol. 7, no. 2, pp. 17-26, June 2013.

[3] S. Yang, A. Bryant, et al., "An industry-based survey of reliability in power electronic converters," *IEEE Trans. Ind. Appl.*, vol. 47, no. 3, pp. 1441-1451, May-June 2011.

[4] B. Lu and S. K. Sharma, "A literature review of IGBT fault diagnostic and protection methods for power inverters," *IEEE Trans. Ind. Appl.*, vol. 45, no. 5, pp. 1770-1777, July 2009.

[5] Meireles M G, Almeida P M, Simoes M G, "A comprehensive review for industrial applicability of artificial neural networks", *IEEE Trans. Ind. Electron.*, vol. 50, no. 3, pp. 585-601, June 2003.

[6] J. F. Martins, V. F. Pires, and A. J. Pires, "Unsupervised neural-network-based algorithm for an on-line diagnosis of three-phase induction motor stator fault", *IEEE Trans. Ind. Electron.*, vol. 54, no. 1, pp. 259-264, June 2007.

[7] S. Khomfoi and L. M. Tolbert, "Fault diagnostic system for a multilevel inverter using a neural network", *IEEE Trans. Power Electron.*,vol. 22, no. 3, pp. 1062–1069, May 2007.

[8] Mamat M R, Rizon M, Khanniche M S. "Fault detection of 3-phase VSI using wavelet-fuzzy algorithm". *American Journal of Applied Sciences*, vol. 3, no. 1, pp. 1642-1648, 2006.

[9] Hu Zhikun, Gui Weihua, Yang Chunhua, et al., "Fault classification method for inverter based on hybrid support vector machines and wavelet analysis", *International Journal of Control, Automation and Systems*, vol. 9, no. 7, pp. 797-804, Aug. 2011.

[10] Cherif B E, Bendiabdellah A. "Detection of two-level inverter open-circuit fault using a combined DWT-NN approach", *Journal of Control Science & Engineering*, no. 3, pp. 1-11, Mar. 2018.

[11] Y. Wang, Z. Li, M. Xu, et al., "A comparative study of two diagnostic methods based on switching voltage pattern for IGBTs open-circuit faults in voltage-source inverters," *J. Power Electron.*, vol. 16, no. 3, pp. 1087-1096, 2016.

[12] Rodríguez-Blanco M A, Vazquez-Perez A, et al., "Fault detection for IGBT using adaptive thresholds during the turn-on transient", *IEEE Trans. Ind. Electron.*, vol. 62, no. 3, pp. 1975-1983, Mar. 2015.

[13] Z. Li, Y. Wang, H. Ma, L. Hong, "Open-transistor faults diagnosis in voltage-source inverter based on phase voltages with sliding-window counting method". in *Proc. 42nd IEEE IECON.*, 2016, pp. 435-440.

[14] Wang Y, Li Z, Lin L. "A novel diagnosis method based on flexible error voltage for IGBTs open-circuit faults in voltage-source inverters", in *Proc. 41st IEEE IECON*, 2015, pp. 19-24.

[15] Estima, J.O. and A.J. Marques Cardoso, "A New Approach for Real-Time Multiple Open-Circuit Fault Diagnosis in Voltage-Source Inverters", *IEEE Trans. Ind. Appl.*, vol. 47, no. 6, pp. 2487-2494, Nov. 2011.

[16] Diallo D, Benbouzid M E H, Hamad D, et al., "Fault detection and diagnosis in an induction machine drive: A pattern recognition approach based on concordia stator mean current vector", *IEEE Trans. Energy Conversion*, vol. 20, no. 3, pp. 512-519, Sept. 2005.

[17] Estima J O, Cardoso A J M., "A new algorithm for real-time multiple open-circuit fault diagnosis in voltage-fed PWM motor drives by the reference current errors", *IEEE Trans. Ind. Electron.*, vol. 60, no. 8, pp. 3496-3505, Aug. 2013.

[18] Choi J H, Kim S, Yoo D S, et al., "A diagnostic method of simultaneous open-switch faults in inverter-fed linear induction motor drive for reliability enhancement", *IEEE Trans. Ind. Electron.*, vol. 62, no. 7, pp. 4065-4077, July 2015.

[19] An Q T, Sun L, Sun L Z., "Current residual vector-based open-switch fault diagnosis of inverters in PMSM drive systems", *IEEE Trans. Power Electron.*, vol. 30, no. 5 pp. 2814-2827, May 2015.

[20] Zhang H, Li Z, Liu J, et al. "Voltage vector error fault diagnosis for open-circuit faults of three-phase four-wire active power filters", *IEEE Trans. Power Electron.*, vol. 32, no. 3, pp. 2215-2226, Mar. 2017.

[21] Jlassi I, Estima J O, El Khil S K, et al., "Multiple open-circuit faults diagnosis in back-to-back converters of PMSG drives for wind turbine systems", *IEEE Trans. Power Electron.*, vol. 30, no. 5, pp. 2689-2702, May 2015.

[22] Z. Li, H. Ma, Z. Bai, Y. Wang and B. Wang, "Fast transistor open-circuit faults diagnosis in grid-tied three-phase VSIs based on average bridge arm pole-to-pole voltages and error-adaptive thresholds", *IEEE Trans. Power Electron.*, vol. 33, no. 9, pp. 8040-8051, Sept. 2018.

[23] Yetendje, Alain, et al., "Sensor fault tolerant control of a magnetic levitation system." *International Journal of Robust and Nonlinear Control*, vol. 20, no.18, pp. 2108-2121, Nov. 2010.

[24] El Khil S K, Jlassi I, Estima J O, et al. "Current sensor fault detection and isolation method for PMSM drives using average normalised currents", *Electronics Letters*, vol. 52, no. 17, pp. 1434-1436, July 2016.

[25] Gou B, Ge X L, Liu Y C, et al., "Load-current-based current sensor fault diagnosis and tolerant control scheme for traction inverters", *Electronics Letters*, vol. 52, no. 20, pp. 1717-1719, Sept. 2016.

[26] H. Berriri, M. W. Naouar and I. Slama-Belkhodja, "Easy and fast sensor fault detection and isolation algorithm for electrical drives," *IEEE Trans. Power Electron.*, vol. 27, no. 2, pp. 490-499, Feb. 2012.

[27] Youssef A B, El Khil S K, Slama-Belkhodja I., "State observer-based sensor fault detection and isolation, and fault tolerant control of a single-phase PWM rectifier for electric railway traction", *IEEE Trans. Power Electron.*, vol. 28, no. 12, pp. 5842-5853, May 2013.

[28] Yu Y, Zhao Y, Wang B, et al., "Current sensor fault diagnosis and tolerant control for VSI-based induction motor drives", *IEEE Trans. Power Electron.*, vol. 33, no. 5, pp. 4238-4248, May 2018.

[29] Papadopoulos P M, Hadjidemetriou L, et al., "Robust fault detection, isolation, and accommodation of current sensors in grid side converters", *IEEE Trans. Ind. Appl.*, vol. 53, no. 3, pp. 2852-2861, Dec. 2017.

[30] Xia J, Guo Y, Dai B, et al., "Sensor fault diagnosis and system reconfiguration approach for an electric traction PWM rectifier based on sliding mode observer", *IEEE Trans. Ind. Appl.*, vol. 53, no. 5, pp. 4768-4778, June 2017.

[31] Jlassi, Imed, et al., "A robust observer-based method for IGBTs and current sensors fault diagnosis in voltage-source inverters of PMSM drives," *IEEE Trans. Ind. Appl.*, vol. 53, no. 3, pp. 2894-2905. May-June 2017.

[32] Y. Ren, Z. Li, B. Wang, Z. Bai and H. Ma, "A fast average model-based method for IGBT and current sensor fault diagnosis in grid-tied inverters," in *Proc. 44th IEEE IECON*, 2018, pp. 3809-3814.

[33] S. Khojet el khil, et al., "Diagnosis of open-switch and current sensor faults in PMSM drives, through stator current analysis," *IEEE Trans. Ind. Appl.*, 2019. Doi: 10.1109/TIA.2019.2930592

[34] Z. Li, B. Wang, Y. Ren, et al.,"L and LCL filtered grid-tied single-phase inverter transistor open-circuit fault diagnosis based on post-fault reconfiguration algorithms", *IEEE Trans. Power Electron.*, vol. 34, no. 10, pp. 10180-10192, Oct. 2019.

Zhan Li (S'16) was born in 1992. He received the B.S. degree and Ph.D. degree in Electrical Engineering from Zhejiang University, Hangzhou, China, in 2014 and 2019 respectively. He was a visiting student in the Power Electronics, Machines and Control Group group, University of Nottingham, UK, from Sept. 2018 to Feb. 2019. Since Sep. 2019, he has been with Nanyang Technological University, Singapore, as a research fellow.

His current research interests include control algorithms, fault diagnosis, and tolerance for power converters.

Pat Wheeler (M'00–SM'12) received his BEng [Hons.] degree in 1990 from the University of Bristol, UK. He received his PhD degree in Electrical Engineering for his work on Matrix Converters from the University of Bristol, UK in 1994.

In 1993 he moved to the University of Nottingham and worked as a research assistant in the Department of Electrical and Electronic Engineering. In 1996 he became a Lecturer in the Power Electronics, Machines and Control Group at the University of Nottingham, UK. Since January 2008 he has been a Full Professor in the same research group.

Dr. Wheeler was Head of the Department of Electrical and Electronic Engineering at the University of Nottingham from 2015 to 2018. He is currently the Head of the Power Electronics, Machines and Control Research Group; Global Director of the University of Nottingham's Institute of Aerospace Technology and is the Li Dak Sum Chair Professor in Electrical and Aerospace Engineering. He is a member of the IEEE PELs AdCom and was an IEEE PELs Distinguished Lecturer from 2013 to 2017. He has published 500 academic publications in leading international conferences and journals.

Alan Watson (S'03–M'08) received the M.Eng. degree [Hons.] in electronic engineering from the University of Nottingham, UK in 2004, and a PhD, also from the University of Nottingham in 2008. In 2009, he was a Research Fellow with the Power Electronics Machines and Control Group, University of Nottingham, where he was involved in the UNIFLEX project (http://www.eee.nott.ac.uk/uniflex/). Since 2009, he has been involved in various projects in the area of high power electronics including high power resonant converters, high voltage power supplies, and multilevel converters for grid connected applications such as HVDC and Flexible AC Transmission Systems. In 2012, he was promoted to Senior Research Fellow before becoming an Assistant Professor in High Power Electronics in 2013.

His current research interests include the development and control of advanced high power conversion topologies for industrial applications.

Alessandro Costabeber (S'09–M'13) received the MSc degree with honours in Electronic Engineering from the University of Padova, Italy, in 2008 and the Ph.D. in Information Engineering from the same university in 2012, on energy efficient architectures and control for future residential microgrids.

In 2014 he joined the PEMC group at the University of Nottingham, UK as Lecturer in Power Electronics. Since 2019 he is Associate Professor at the University of Padova, Italy. His current research interests include modular multilevel converters for HVDC, high power density converters, control and stability analysis of AC and DC microgrids. Dr. Costabeber received the IEEE Joseph John Suozzi INTELEC Fellowship Award in Power Electronics in 2011. Electronics.

His current research interests include HVDC converters topologies, high power density converters for aerospace applications, control solutions and stability analysis of AC and DC microgrids, control and modelling of power converters, power electronics and control for distributed and renewable energy sources.

Borong Wang (S'19**)** was born in Shandong Province, China, in 1989. He received the B.S. and M.S. degrees from Qingdao University of Technology, Qingdao, China, in 2012 and 2016. He is currently working toward the Ph.D. degree in electrical engineering from Zhejiang University, Hangzhou, China.

His current research interests include the fault diagnosis for power converters and tolerant strategy of multilevel inverter system.

Yini Ren (S'18) was born in Zhejiang, China. She received her B.S. degree in Electrical Engineering from Zhejiang University, Hangzhou, China, in 2017, where she is currently working towards her M.S. degree in Electrical Engineering.

Her current research interests include fault diagnosis of power electronic circuits and grid-tied inverters.

Zhihong Bai (M'09) was born in Shanxi, China. She received the Ph.D. degree in electrical engineering from Zhejiang University, Hangzhou, China, in 2008. Since 2011, she has been with Zhejiang University, where she is currently an Associate Professor in the College of Electrical Engineering.

Her current research interests include renewable energy systems as well as high-power and multilevel converters.

Hao Ma (M'99-SM'18) received the B.S., M.S., and Ph.D. degrees from Zhejiang University, Hangzhou, China, in 1991, 1994 and 1997, respectively, all in electrical engineering.

Since 1997, he has been a Lecturer, Associate Professor, and Professor at Zhejiang University. From September 2007 to September 2008, he was a Delta Visiting Scholar at the North Carolina State University. He is the Vice Dean of the ZJU-UIUC Institute. He has authored two books and has authored or coauthored over 200 technical papers. His current research interests include advanced control in power electronics, wireless power transfer, fault diagnosis of power electronic circuits and systems, and application of power electronics.

Dr. Ma is currently the Director of Academic Committee of China Power Supply Society. He is the Associate Editor of the IEEE Journal of Emerging and Selected Topics in Power Electronics and the Journal of Power Electronics. He was the AdCom member of the IEEE Industrial Electronics Society, the Technical Program Chair of the IEEE ISIE 2012, IEEE PEAC 2014 and IEEE PEAC 2018.